PHYSICOCHEMICAL STUDIES
OF SYSTEMS AND PROCESSES

Co$_3$O$_4$ Nanoparticles Modified TiO$_2$ Nanotube Arrays with Improved Photoelectrochemical Performance[1]

Huazhen Cao[a], Yueheng Lu[a], Wei Ning[a], Huibin Zhang[a], and Guoqu Zheng[a],*

*[a] College of Materials Science and Engineering, Zhejiang University of Technology,
Hangzhou 310014, China
e-mail: Zhenggq@zjut.edu.cn

Abstract—Co$_3$O$_4$ modified TiO$_2$ nanotube arrays (TiO$_2$–NTs) were successfully fabricated by electrodeposition and thermal oxidation process. The prepared samples were characterized by field emission scanning electron microscopy (FESEM), transmission electron microscopic (TEM), X-ray diffraction (XRD), X-ray photoelectron spectroscopy (XPS), and UV-visible diffuse reflectance spectroscopy. The photoelectrocatalytic properties of as-prepared samples were investigated under visible light and UV-vis light irradiation. Meanwhile, taking methyl orange aqueous solution as target substrate for photoelectrocatalytic degradation experiments, the degradation rate under UV-vis light irradiation and dark condition were evaluated. The prepared Co$_3$O$_4$/TiO$_2$–NTs exhibited much higher photoelectrochemical activity than TiO$_2$–NTs under visible light irradiation and UV-vis light irradiation. The degradation rate of methyl orange on Co$_3$O$_4$/TiO$_2$–NTs electrode reaches 90.7% under applied potential of 1.3 V and UV-vis light irradiation for 10 h, which is only 53.4% on TiO$_2$–NTs electrode. The improved performance could be attributed to the higher photo-generated carrier concentration and carrier mobility.

Keywords: TiO$_2$ nanotube arrays, Co$_3$O$_4$ nanoparticles, photoelectrocatalysis, methyl orange degradation

DOI: 10.1134/S1070427219010099

INTRODUCTION

Water pollution has always been a major concern among the environmental issues, most of the pollutants in water are stable in nature. The environmental laws and regulations become more stringent [1], and efficient degradation methods appeal to lots of researchers all over the world. Many reports [2–4] demonstrate that semiconductor heterojunction catalysts can effectively degrade organic pollutants under appropriate conditions. TiO$_2$ nanotube arrays as an *n*-type semiconductor attract tremendous attention because of their unique structure and excellent properties [5, 6], which is widely used in photodegradation [7], sensors [8], hydrogen generation [9], and dye sensitized solar cells [10, 11]. Nevertheless, the intrinsic band gap of TiO$_2$ (3.2 eV for anatase and 3.0 eV for rutile) limits its absorption in the ultraviolet part of solar spectrum [12]. The construction of a heterostructure by metal-oxide-

semiconductor doping on TiO$_2$ is an effective way to solve this issue [13].

Many metal oxides (such as Bi$_2$O$_3$ [14], Co$_3$O$_4$ [15], SnO$_2$ [16], WO$_3$ [17], and ZnO [18]) have been reported to couple with TiO$_2$ to form heterostructured photocatalysts with enhanced photocatalysis. Among them, Co$_3$O$_4$ is one of the most intriguing *p*-type semiconductor materials with two band gaps of 1.5 and 2.2 eV [15]. Up to this day, cobalt oxide thin-film can be prepared by many methods, such as RF sputtering [19], chemical vapor deposition [20], spray pyrolysis [21], and electrodeposition techniques [22]. Numerous studies have proved that a *p-n* junction photocatalysts coupled with other semiconductors is an efficient way to enhance the photocatalytic activity of the Co$_3$O$_4$ [23]. Cao et al. [24] introduced photochemical coating method to prepare Co$_3$O$_4$-modified TiO$_2$ nanorod arrays, which remarkably enhanced visible light photoelectrochemical response in comparison with the pure TiO$_2$–NTs. Fan et al. [25] developed a photodeposition strategy to synthesize Co$_3$O$_4$/TiO$_2$ com-

---

[1] The text was submitted by the authors in English.

posites, which significantly enhanced performance for lithium-ion batteries. Wang et al. [26] prepared Co$_3$O$_4$/ TiO$_2$ nanofibers heterostructure via a simple two-step process including electrospinning and hydrothermal process, and found that the prepared material exhibited a relatively high catalysis response to CO.

In this work, well ordered TiO$_2$ nanotube arrays was coupled with Co$_3$O$_4$ nanoparticles via a simple electrodeposition and thermal oxidation process. The photoelectrocatalytic activity of the prepared Co$_3$O$_4$/TiO$_2$–NTs was evaluated for the degradation of methyl orange. It is aimed to provide a new route to synthesis Co$_3$O$_4$/TiO$_2$–NTs hybrid with excellent photoelectrocatalytic properties under visible light.

EXPERIMENTAL

Material synthesis. TiO$_2$–NTs was prepared on commercial pure titanium substrates (purity 99.95%) by potentiostatic anodization in 1 wt % hydrofluoric solution at 20 V for 20 min [27]. The as-prepared electrode was thoroughly washed by deionized water and then annealed at 450°C for 2 h with heating and cooling rates of 5°C/min in air.

Co$_3$O$_4$ nanoparticles were loaded on TiO$_2$–NTs via electrodeposition followed by thermal oxidation treatments. Electrodeposition was carried out in a solution composed of 0.05 M CoSO$_4$ and 1 M (NH$_4$)$_2$SO$_4$ at current density of –1 mA cm^{-2}. Pt was used as auxiliary electrode. Thermal oxidation was performed at 450°C for 2 h in a quartz tube furnace.

Characterization. The morphology of the as-prepared samples was measured by field-emission scanning electron microscopy (FESEM, Hitachi S-4700) and transmission electron microscopic (TEM, FEI, TecnaiG2F30). X-ray diffraction (XRD) patterns of the TiO$_2$ nanotube were characterized on a PHILIPS Panalytical X'Pert PRO using CuK_α radiation. X-ray photo electron spectroscopy (XPS) measurements were performed on a Kratos AXIS Ultra DLD Xray photoelectron spectrometer system with a AlK_α X-ray source (h = 1486.6 eV). Binding energy values were calibrated by the reference of contaminant carbon (C1s = 284.8 eV). UV-visible diffuse reflectance spectra were obtained on an UV-visible spectrophotometer (UV-2550, Shimadzu, Japan). BaSO$_4$ was used as a reflectance standard.

Photoelectrochemical measurements. The photoelectrochemical properties were investigated in a con-

ventional three-electrode system on CHI660C electrochemical workstation. The prepared sample with exposure area of 1 cm^2, platinum sheet and saturated calomel electrode (SCE) were used as working electrode, counter electrode and reference electrode, respectively. 0.2 M Na$_2$SO$_4$ aqueous solution was used as the electrolyte. A 300 W Xenon lamp (Au Light, CEL-TCX250) with a visible-light filter (>420 nm) was used as light source for the photoelectrochemical measurement.

Photoelectrocatalytic degradation experiments. The photoelectrocatalytic degradation experiments were investigated by using 30 mL methyl orange with an initial concentration of 4 mg L^{-1} as model pollutant in a homemade rectangular glass container (4 cm × 2 cm × 5 cm). One side of the container was quartz glass, so the UV light can get through. A 300W Xenon lamp (Au Light, CEL-TCX250) was positioned 10 cm away from the container and the light intensity reaching the surface of sample was about 18 mW cm^{-2}. The photoelectrochemical degradation reactions were carried out at applied potential of 1.3 V under UV-vis light irradiation. The concentration of methyl orange was analyzed using UV-visible spectrophotometer at wavelength of 462.5 nm.

RESULTS AND DISCUSSION

Characterization of Co$_3$O$_4$/TiO$_2$–NTs. The morphologies of TiO$_2$–NTs and Co$_3$O$_4$/TiO$_2$–NTs were observed by SEM and TEM. Figure 1a is a typical SEM image of TiO$_2$–NTs obtained by anodic oxidation, which reveals a regularly arranged tubular structure. Figure 1b shows the surface morphology of Co$_3$O$_4$/TiO$_2$–NTs. It can be seen that most Co$_3$O$_4$ was deposited into the pore space of TiO$_2$–NTs successfully, only few spherical Co$_3$O$_4$ nanoparticles was grown on the surface of TiO$_2$– NTs. Figure 1c is the TEM image of Co$_3$O$_4$/TiO$_2$–NTs, in which the TiO$_2$ nanotubes are clearly visible and the deposits are located in both the inner side of nanotubes and the gap between nanotubes.

Figure 2 shows the XRD pattern of the prepared Co$_3$O$_4$/TiO$_2$–NTs. The diffraction peaks of Ti are clearly seen because Ti is a substrate with high crystallinity and the thick of layer is only several hundred nanometers. The peak emerging at 25.28° is attributed to the (101) reflection of anatase phase TiO$_2$ (JCPSD, no. 71-1166). And the peak at 36.82° corresponds to the (311) of cubic phase Co$_3$O$_4$ (JCPSD, no. 73-1701). No other diffraction
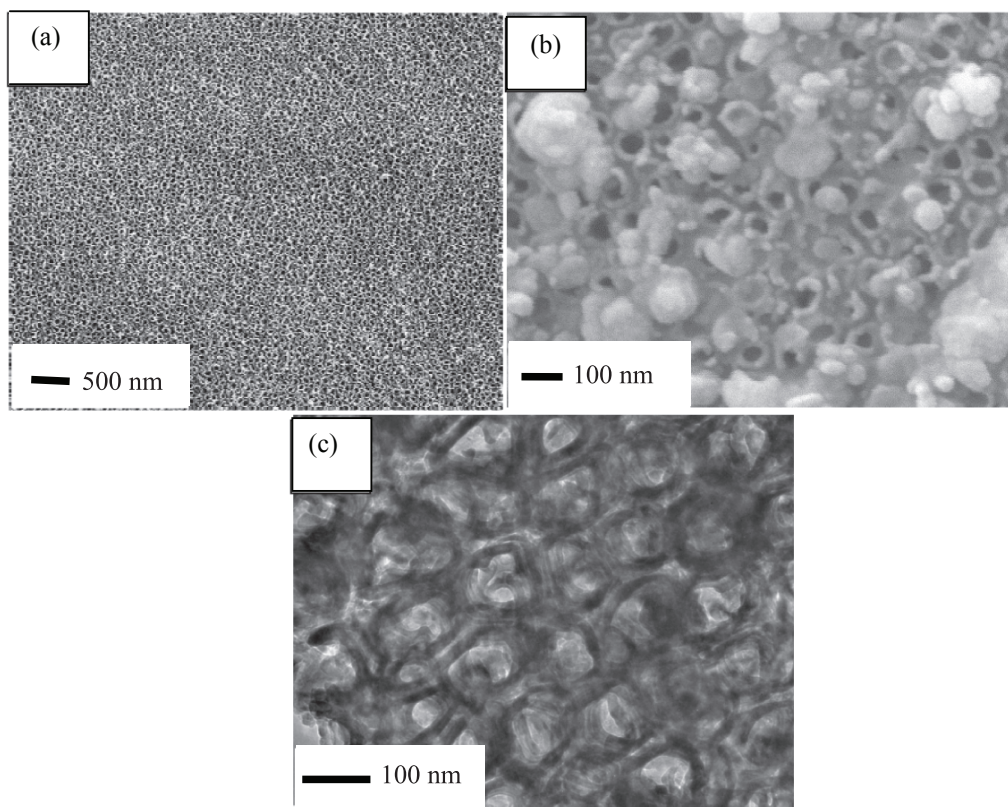
Fig. 1. SEM images of (a) TiO_2–NTs, (b) Co_3O_4/TiO_2–NTs, and (c) TEM image of Co_3O_4/TiO_2–NTs.

peaks could be detected. XRD analysis indicates that heat treatment enables a complete transformation of the electrodeposited cobalt to Co_3O_4, after which Co_3O_4/TiO_2–NTs nanostructured electrode was obtained.
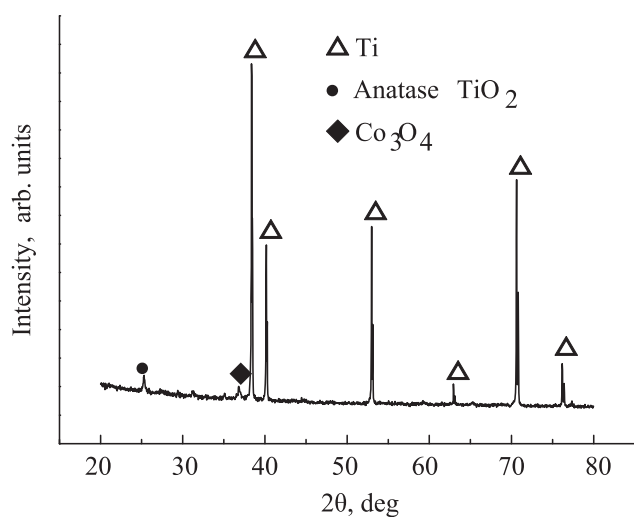
X-ray photo electron spectroscopy was measured to further determine the valence state of Co in the prepared sample. Figure 3 represents the XPS spectrum of Co2p, from which we can find that the main Co2p
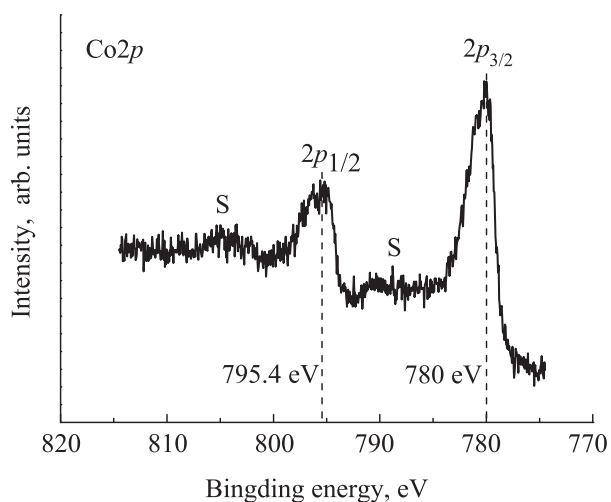

Fig. 2. XRD pattern of Co_3O_4/TiO_2–NTs.

Fig. 3. XPS spectra of the Co2p binding energy region of Co_3O_4/TiO_2–NTs.
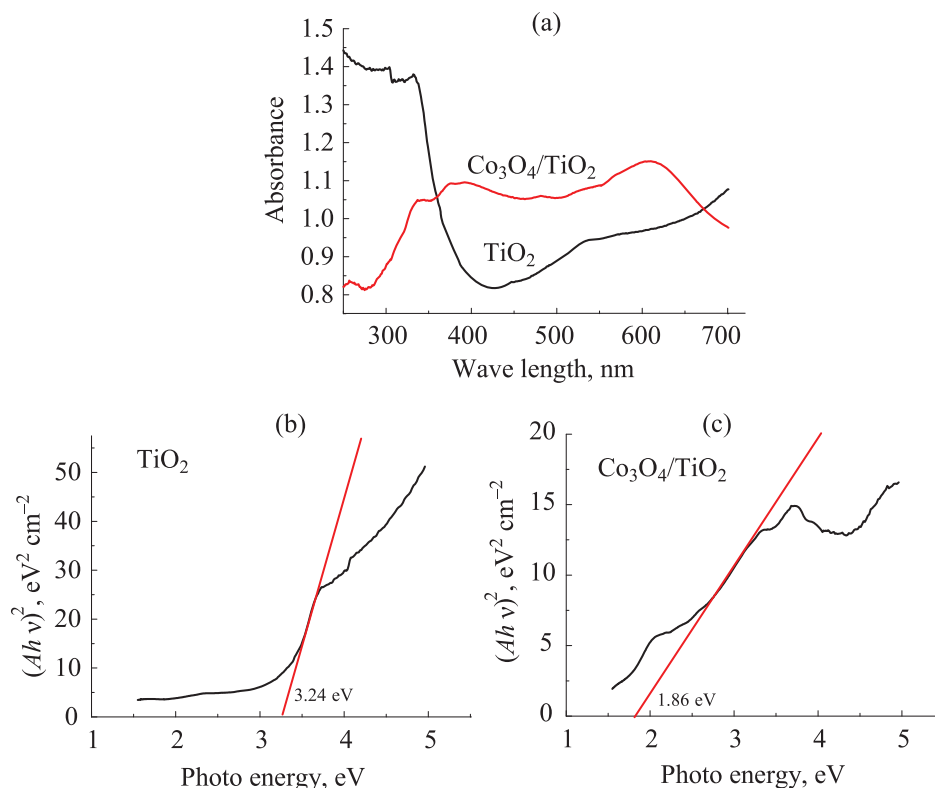
Fig. 4. (Color online) (a) UV-vis diffuse reflection spectra of TiO$_2$–NTs and Co$_3$O$_4$/TiO$_2$–NTs, (b) and (c) plot analysis of optical band gap of TiO$_2$–NTs and Co$_3$O$_4$/TiO$_2$–NTs, respectively

photoelectron peaks are located at 780 and 795.4 eV with two shake-up satellite peaks at about 788.7 and 804.8 eV. The emerged peaks indicate that the Co is in the form of trivalence, corresponding well with Co$_3$O$_4$ [28, 29], i.e. the synthesized sample is Co$_3$O$_4$/TiO$_2$–NTs.

UV-vis diffuse reflection spectra. Figure 4 shows the UV-vis diffuse reflectance spectra of TiO$_2$–NTs and Co$_3$O$_4$/TiO$_2$–NTs. It is apparent that Co$_3$O$_4$/TiO$_2$–NTs exhibits an enhanced absorption in all visible and part of the ultraviolet region compared with TiO$_2$–NTs. However, TiO$_2$–NTs showed a higher absorption in most ultraviolet region.

The energy band gap (E_g) can be estimated by the Tauc equation [30]:

$$\alpha h\nu = C(h\nu - E_g)^n, \qquad (1)$$

where $h\nu$ is the photon energy, C is the constant, α is the absorption coefficient, $n = 2$ for an indirect bandgap semiconductor and $n = 1/2$ for a direct bandgap semiconductor. The E_g is calculated by a linear fit to the experimental $(\alpha h\nu)^2$ vs. $h\nu$ plot. The intersection point of the tangent and horizontal ordinate is the E_g. It can

be seen from Fig. 4 that the E_g of Co$_3$O$_4$/TiO$_2$–NTs is 1.86 eV, whereas the E_g of TiO$_2$–NTs is 3.24 eV. This result also indicates that the TiO$_2$ in this case has an anatase crystal, which is basically consistent with the XRD results. The valance band edge position of Co$_3$O$_4$/TiO$_2$–NTs heterostructure can be estimated by a simple approach. The valence band potential at the point of zero charge was calculated by the following equation [31]:

$$E_{VB} = X - E^e + 0.5E_g, \qquad (2)$$

where E_{VB} is the valence band edge potential, X is the geometric mean of the absolute electronegativity of the constituent atoms, E^e is the energy of free electrons on the hydrogen scale (about 4.5 eV), and the conduction band potential (E_{CB}) can be determined by $E_{CB} = E_{VB} - E_g$. The X values for TiO$_2$ and Co$_3$O$_4$ are 5.81 and 5.93 eV, the E_{VB} of TiO$_2$–NTs and Co$_3$O$_4$ are calculated to be 2.93 and 2.36 eV, respectively. Therefore, the E_{CB} of TiO$_2$–NTs and Co$_3$O$_4$ are estimated to be –0.31 and 0.50 eV.

A schematic diagram for the photo-generated charge separation of Co$_3$O$_4$/TiO$_2$–NTs heterostructure is established, as shown in Fig. 5. When the p–n
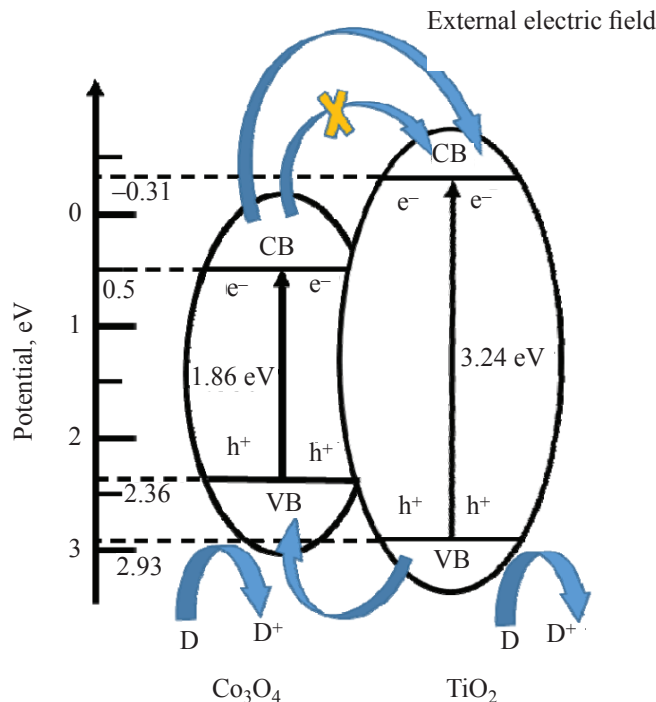
Fig. 5. (Color online) Schematic diagram for the photo-generated charge separation of Co_3O_4/TiO_2–NTs.

junction is formed, the free electrons of the *n*-type semiconductor (TiO_2) are combined with the holes of *p*-type semiconductor (Co_3O_4). At this time, the *p*-type semiconductor is negatively charged, and the *n*-type semiconductor is positively charged, thereby forming an internal electric field from the *n*-type TiO_2 to *p*-type Co_3O_4. According to the band edge position, photo-generated holes on the valence band (VB) of *n*-type TiO_2 can transfer to *p*-type Co_3O_4 easily [32], while the photogenerated electrons on the conduction band (CB) can not transfer from Co_3O_4 to TiO_2 without the aid of external electric field.

Photoelectrochemical performance. Figure 6 shows the photocurrent densities of TiO_2–NTs and Co_3O_4/TiO_2–NTs measured under visible light illumination and UV-vis light illumination in 0.2 M Na_2SO_4 solution. Under visible light irradiation, the photoresponse on TiO_2–NTs is very weak because TiO_2–NTs can hardly absorb visible light due to its wide intrinsic band gap. While for the case of Co_3O_4/TiO_2–NTs, there is a significant improvement in the photoelectrochemical performance, which is evidenced by the enhanced photocurrent. As Fig. 5 demonstrates, the Co_3O_4 nanoparticles has narrow bandgap close to the energy of visible light, so it can be excited by sunlight. At the

same time, the Co_3O_4 and TiO_2–NTs form a *p-n* junction, which benefits the separation of photon-generated carriers and then leads to a higher photocurrent density. It is also found that with the increase in applied potential, the photocurrent of Co_3O_4/TiO_2–NTs increased rapidly, while the photocurrent of TiO_2–NTs had no evident changes. For TiO_2–NTs, carrier mobility reached a maximum value under a low potential and the concentration of photo-generated carrier were lower. Co_3O_4/TiO_2–NTs were in a different situation, not only for its higher photo-generated carrier concentration, but also for its increasing carrier mobility.

The responses of the TiO_2–NTs and Co_3O_4/TiO_2–NTs under UV-vis light irradiation are shown in Fig. 5b. Different from visible light irradiation, TiO_2–NTs exhibit an obvious absorption in ultraviolet region. When the applied potential is lower than 0.8 V, Co_3O_4/TiO_2–NTs hybrid does not show comparative advantage compared with TiO_2–NTs. However, when the applied potential is greater than 0.8 V, the existence of Co_3O_4 nanoparticles significantly enhanced its photoelectrochemical performance. As previously stated, carrier mobility reached a maximum value under a low potential for TiO_2–NTs, so its photocurrent has no evident changes with the increase in applied potential. It is found that the doping of
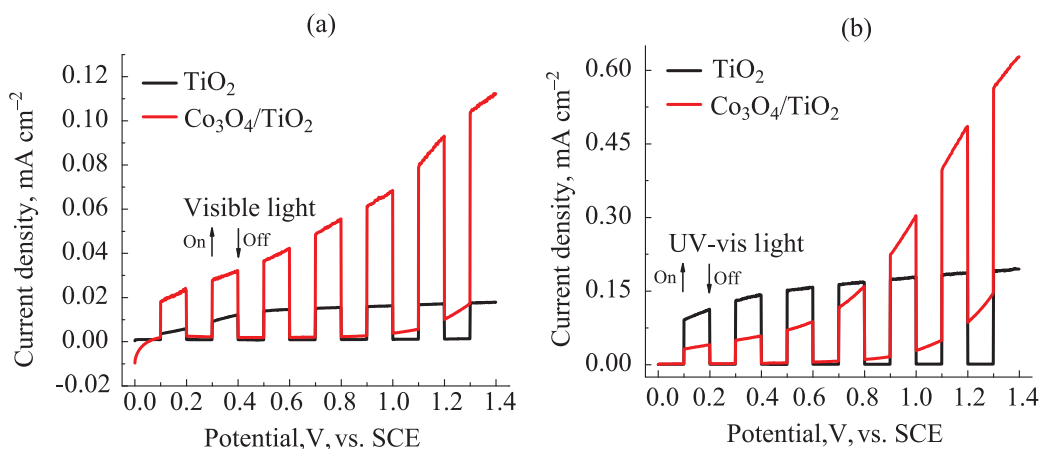
Fig. 6. (Color online) Photocurrent vs. potential curves for TiO$_2$–NTs and Co$_3$O$_4$/TiO$_2$–NTs in 0.2 M Na$_2$SO$_4$ solution under (a) visible light illumination and (b) UV-vis light illumination.

Co$_3$O$_4$ nanoparticles into TiO$_2$–NTs causes the photocurrent decay to some extent at low potential, which may be owing to the lower carrier mobility in Co$_3$O$_4$ nanoparticles and the photo-generated carriers in Co$_3$O$_4$ nanoparticles are easy to recombination in this condition. However, carrier mobility increases significantly with the increase of the potential for the Co$_3$O$_4$/TiO$_2$–NTs sample, that's why the photocurrent density of Co$_3$O$_4$/TiO$_2$–NTs reached 0.56 mA cm^{-2} when potential is 1.3 V, approximately three times higher than TiO$_2$–NTs.

Photoelectrocatalytic degradation methyl orange. Photoelectrocatalytic degradation methyl orange was conducted to evaluate the performance of the prepared Co$_3$O$_4$/TiO$_2$–NTs. Figure 7 displays the degradation curves of methyl orange on different samples under UV-vis light illumination with applied potential of 1.3 V. For comparison, the degradation experiment under dark condition is also conducted. It is found that both TiO$_2$–NTs and Co$_3$O$_4$/TiO$_2$–NTs show a significantly enhancement in degradation rate under UV-vis light illumination. Co$_3$O$_4$/TiO$_2$–NTs displays a superior photoelectrocatalytic activity, and 90.7% of methyl orange molecules are degraded under UV-vis light irradiation for 10 h. In contrast, only 53.4% of methyl orange molecules are degraded by TiO$_2$–NTs.

CONCLUSIONS

In summary, Co$_3$O$_4$ modified TiO$_2$ nanotube arrays (TiO$_2$–NTs) were successfully fabricated by electrodeposition and thermal oxidation process. The photoelectro-

chemical performance of TiO$_2$–NTs and Co$_3$O$_4$/TiO$_2$–NTs were measured under visible light illumination and UV-vis light illumination. The existence of Co$_3$O$_4$ nanoparticles significantly enhances the visible light response. When the applied potential is lower than 0.8 V, Co$_3$O$_4$/TiO$_2$–NTs hybrid does not show comparative advantage compared with TiO$_2$–NTs. While at potential greater than 0.8 V, the doping of Co$_3$O$_4$ nanoparticles significantly enhances its photoelectrochemical performance under UV-vis light irradiation. The degradation rate of methyl orange on Co$_3$O$_4$/TiO$_2$–NTs electrode
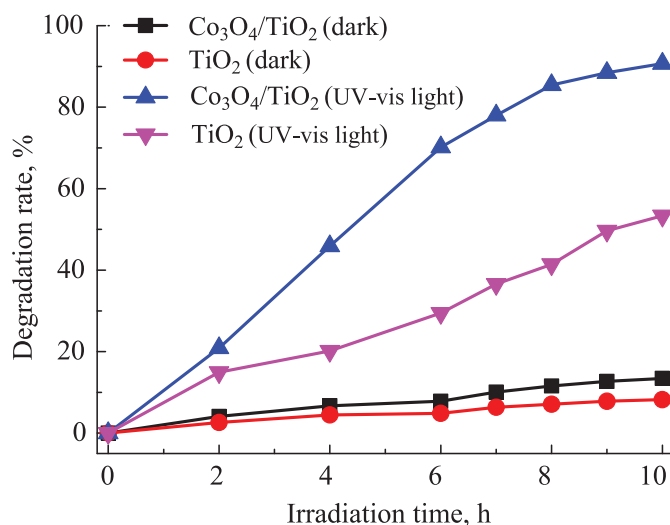

Fig. 7. (Color online) Photoelectrochemical degradation curves of methyl orange on samples under UV-vis light illumination and dark condition with 1.3 V potential.

reaches 90.7% under applied potential of 1.3 V and UV-vis light irradiation for 10 h, which is only 53.4% on TiO_2–NTs electrode. The improved performance could be attributed to the higher photo-generated carrier concentration and carrier mobility.

FUNDING

REFERENCES

1. Gogate, P.R. and Pandit, A.B., *Adv. Env. Res.,* 2004, vol. 8(3), pp. 501–551.

2. Li, D.D., *Chinese J. Inorg. Chem.*, 2012, vol. 28(7), pp. 1343–1347.

3. Li, J., Zhao, H., Lei, Y., Lei, Q., and Zheng, Z., *Nano*, 2018, vol. 13(4):1850045.

4. Ranjit, K.T., Willner, I., Bossmann, S.H., and Braun, A.M., *J. Materials Sci.,* 1999, vol. 34(21), pp. 5273–5280.

5. Rho, W.Y., Kim, H.S., Sang, H.L., Jung, S., Suh, J.S., Hahn, Y.B., and Jun., B.H., *Chem. Physics Letters*, 2014, vol. 614, pp. 78–81.

6. Tang, Y., Hong, L., Li, J., Hou, G., Cao, H., Wu, L., Zheng, G., and Wu, Q., *Chem. Commun*, 2017, vol. 53(38), pp. 5298–5301.

7. Jiang, F., Zheng, S.R., Zheng, Z., Xu, Z.Y., and Wang., Y.J., *J. Env. Sci.,* 2006, vol. 18(4), pp. 783–787.

8. Yang, J., Li, D., Pang, Z., and Wei, Q., *Nano*, 2016, vol. 11(12), p. 1650132.

9. Cheng, X., Lu, Y., Gu, S., and Dawson, G., *Nano*, 2017, vol. 12(9), p. 1750115.

10. Kuang, D., Brillet, J., Chen, P., Takata, M., Uchida, S., Miura, H., Sumioka, K., Zakeeruddin, S.M., and Grätzel, M., *Acs Nano*, 2008, vol. 2(6), pp. 1113–1116.

11. Roy, P., Kim, D., Lee, K., Spiecker, E., and Schmuki, P., *Nanoscale*, 2010, vol. 2(1), pp. 45–59.

12. Zhong, J.S., Wang, Q.Y., and Yu, Y.F., *J. Alloys & Compounds*, 2015, vol. 620(0), pp. 168–171.

13. Santamaria, M., Conigliaro, G., Franco, F.D., and Quarto, F.D., *Electrochimica Acta*, 2014, vol. 144(0), pp. 315–323.

14. Bessekhouad, Y., Robert, D., and Weber, J.V., *Catalysis Today*, 2005, vol. 101(3), pp. 315–321.

15. Kim, H.K., Seong, T.Y., Lim, J.H., Cho, W.I., and Yoon, Y.S., *J. Power Sources*, 2001, vol. 102(1), pp. 167–171.

16. Hou, L.R., Yuan, C.Z., and Peng, Y., *J. Hazardous Materials*, 2007, vol. 139(2), pp. 310–315.

17. Murakami, Y., Ohta, I., Hirakawa, T., and Nosaka, Y., *Chem. Phys. Letters*, 2010, vol. 493(4), pp. 292–295.

18. Wang, N., Sun, C., Zhao, Y., Zhou, S., Chen, P., and Lei, J., *J. Materials Chem.*, 2008, vol. 18(33), pp. 3909–3911.

19. Lohaus, C., Morasch, J., Brötz, J., Klein, A., and Jaegermann, W., *J. Physics D Appl. Physics*, 2016, vol. 49(15), p. 155306.

20. Mane, A.U., Shalini, K., and Shivashankar, S.A., *J. de Physique IV*, 2001, vol. 11(11), pp. 637–643.

21. Shinde, V.R., Mahadik, S.B., Gujar, T.P., and Lokhande, C.D., *Appl. Sur. Sci.*, 2006, vol. 252(20), pp. 7487–7492.

22. Szmaja, W., Kozłowski, W., Polański, K., Balcerski, J., Cichomski, M., Grobelny, J., Zieliński, M., and Miękoś, E., *Chem. Physics Letters*, 2012, vol. 542(2–3), pp. 117–122.

23. Jang, J.S., Kim, H.G., and Lee, S.H., *J. Physics & Chem. of Solids*, 2012, vol. 73(11), pp. 1372–1377.

24. Cao, C., Hu, C., Shen, W., Wang, S., Wang, J., and Tian, Y.S., *J. Alloys and Compounds*, 2013, vol. 550(0), pp. 137–143.

25. Fan, Y., Zhang, N., Zhang, L., Shao, H., Wang, J., Zhang, J.Q., and Cao, C., *Electrochimica Acta*, 2013. 94(0), pp. 285–293.

26. Wang, L., Deng, J., Lou, Z., and Zhang. T., *J. Materials Chem. A*, 2014, vol. 2(26), p. 10022.

27. Cao, H., Wang, Z., Hou, G., and Zheng, G., *Sur. & Coat. Techn.*, 2010, vol. 205(3), pp. 885–889.

28. Chuang, T.J., Brundle, C.R., and Rice, D.W., *Surface Sci.*, 1976, vol. 59(2), pp. 413–429.

29. Langell, M.A., Anderson, M.D., Carson, G.A., Peng, L., and Smith, S., *Phys. Rev. B Condensed Matter*, 1999, vol. 59, pp. 4791–4798.

30. Peng, H., Lu, J., Wu, C., Yang, Z., Chen, H., Song, W., and Li, P., Yin, H., *Appl. Sur. Sci.*, 2015, vol. 353, pp. 1003–1012.

31. Zhang, X., Zhang, L., Xie, T., and Wang, D., *J. Phys. Chem. C,* 2009, vol. 113(17), pp. 7371–7378.

32. Long, M., Cai, W., Cai, J., Zhou, B., Chai, X., and Wu., Y., *J. Phys. Chem. B*, 2007, vol. 38(4), p. 20211.